applied sciences

MDPI

Article

A Validation Method for EPID In Vivo Dosimetry Algorithms

Marco Esposito [1], Livia Marrazzo [2,*], Eleonora Vanzi [3], Serenella Russo [1], Stefania Pallotta [2,4] and Cinzia Talamonti [2,4]

[1] Medical Physics Unit, Azienda USL Toscana Centro, 50100 Florence, Italy; marco1.esposito@uslcentro.toscana.it (M.E.); serenella.russo@uslcentro.toscana.it (S.R.)
[2] Medical Physics Unit, Careggi University Hospital, 50100 Florence, Italy; stefania.pallotta@unifi.it (S.P.); cinzia.talamonti@unifi.it (C.T.)
[3] Medical Physics Unit, Azienda Ospedaliera Universitaria Senese, 53100 Siena, Italy; eleonora.vanzi@ao-siena.toscana.it
[4] Department of Experimental and Clinical Biomedical Sciences "Mario Serio", University of Florence, 50100 Florence, Italy
* Correspondence: livia.marrazzo@unifi.it; Tel.: +39-055-7946971

Featured Application: Transit dosimetry, with Electronic Portal Imaging Device (EPID), is a powerful tool for in vivo dosimetry (IVD). Despite its wide availability and its simplicity of use, the clinical implementation of such a dosimetric technique is still challenging. One reason for the difficulty of IVD implementation is the lack of guidelines around the validation and acceptance of EPID IVD algorithms. In this paper we propose an evaluation method for assessing the accuracy of a novel 3D EPID back-projection algorithm for IVD. To the best of our knowledge, the EPID back-projection algorithms have never been validated in anthropomorphic phantom against direct two-dimensional measurements, and the new algorithm, introduced in version 5.8 of the Dosimetry Check software for dealing with tissue inhomogeneity, has never been evaluated before.

Abstract: The aim of this study was to develop and apply an evaluation method for assessing the accuracy of a novel 3D EPID back-projection algorithm for in vivo dosimetry. The novel algorithm of Dosimetry Check (DC) 5.8 was evaluated. A slab phantom homogeneously filled, or with air and bone inserts, was used for fluence reconstruction of different squared fields. VMAT plans in different anatomical sites were delivered on an anthropomorphic phantom. Dose distributions were measured with radiochromic films. The 2D Gamma Agreement Index (GAI) between the DC and the film dose distributions (3%, 3 mm) was computed for assessing the accuracy of the algorithm. GAIs between films and TPS and between DC and TPS were also computed. The fluence reconstruction accuracy was within 2% for all squared fields in the three slabs' configurations. The GAI between the DC and the film was 92.7% in the prostate, 92.9% in the lung, 96.6% in the head and the neck, and 94.6% in the brain. An evaluation method for assessing the accuracy of a novel EPID algorithm was developed. The DC algorithm was shown to be able to accurately reconstruct doses in all anatomic sites, including the lung. The methodology described in the present study can be applied to any EPID back-projection in vivo algorithm.

Keywords: in vivo dosimetry; EPID; end-to-end test; anthropomorphic phantom

Citation: Esposito, M.; Marrazzo, L.; Vanzi, E.; Russo, S.; Pallotta, S.; Talamonti, C. A Validation Method for EPID In Vivo Dosimetry Algorithms. *Appl. Sci.* **2021**, *11*, 10715. https://doi.org/10.3390/app112210715

Academic Editor: Qi-Huang Zheng

Received: 7 October 2021
Accepted: 9 November 2021
Published: 13 November 2021

1. Introduction

In vivo dosimetry (IVD) measures how accurately the planned dose is delivered to the patients during radiotherapy treatment. For many years, it has been viewed only as supplementary to a standard clinical QA program, but recently its role in preventing delivery failures and increasing patient safety and treatment quality has been considered. International organizations recommend its use [1] and national and international regulators are starting to require it in national law [2].

Transit dosimetry, with the Electronic Portal Imaging Device (EPID), is a powerful tool for IVD measurements. It enables large scale acquisitions with a relatively low cost for patients and institutes [3]. Many software programs, some of which are commercially available, have been developed in the last ten years that enable the reconstruction of the dose absorbed in the patient's anatomy (in the planning CT or/and in the daily CBCT) either in a point, a plane, in 3D, or even in 4D [4,5]. Despite its wide availability and its simplicity of use, the clinical implementation of such a dosimetric technique is still challenging. Currently, only a few centers have reported wide statistics of IVD results [6,7]. One reason for the IVD implementation difficulty is the lack of guidelines around the validation and acceptance of an EPID IVD algorithm. Moreover, there is no consensus about the dose difference metric and the tolerance levels to use to guarantee the needed level of accuracy and specificity in the errors' detection. The accuracy evaluation of the EPID dose reconstruction algorithm is important for setting the tolerance levels in order to limit the presence of false-positive errors due to algorithm failure. In a recent SBRT study, it was found that, with the standard tolerance levels [8], about 40% of fractions resulted over the tolerance level (OTL), of which approximately half were due to algorithm failure [9]. The presence of tissue inhomogeneity can further increase false-positive errors. Mijnheer et al. found that 34% of OTL but only 1.5% of alerted plans underwent corrective action [10], and the OTL majority was due to EPID algorithm failure in dealing with tissue inhomogeneity.

EPID reconstruction algorithms have been usually validated against absolute dose measurements only in points [11], and the dose distributions were generally compared to the treatment planning system (TPS) computed dose. Only a few studies have validated the EPID reconstructed dose distributions by comparing them with absolute dose measurements [4,12,13]. However, in these studies, the measurements were performed in homogeneous phantoms with simple cylindrical [13] or octagonal [12] geometries.

To the best of our knowledge, the EPID back-projection algorithms have never been validated in an anthropomorphic phantom against direct two-dimensional measurements.

In this work, we assessed the accuracy of the new version of the commercial EPID software, Dosimetry Check (DC). The evaluation was conducted in two steps: first, the capability to reconstruct squared field fluence on slab phantoms with air and bone inhomogeneities was evaluated. In the second phase, the dose distributions reconstructed by DC were compared with radiochromic film dosimetry in the anthropomorphic Alderson Rando phantom for volumetric modulated arc therapy (VMAT) plans. To our knowledge, the new algorithm, introduced in version 5.8 of the DC software for dealing with tissue inhomogeneity, has never been evaluated before.

There is extensive literature about the implementation of EPID software for transit dosimetry in clinical practice. However, this study contains some innovations. In fact, this is the first study comparing EPID based dosimetric results with film dosimetry in an anthropomorphic phantom.

The methodologies shown in this work are the final step of the commissioning of an EPID transit dosimetry system and can be used to validate any back-projection EPID algorithm [6,14] before clinical implementation.

2. Materials and Methods

DC is a back-projection EPID in vivo dosimetry software composed of two independent algorithms. The deconvolution kernel reconstructs the entrance fluence from the EPID image, then the dose computation algorithm uses the reconstructed fluence to compute the dose inside the patient's anatomy. The new 5.8 version of DC contains, in addition to the pencil beam algorithm (PB), a collapsed cone convolution algorithm (CCC) for dose calculation. Moreover, an optimized deconvolution kernel for dealing with tissue inhomogeneities has been implemented. The previous DC version was equipped with only the PB algorithm, the results of which have been reported in previous studies [4,6]. Compared to PB, the dosimetric advantage of the CCC algorithm, in the case of tissue inhomogeneity, is

well documented [15]. However, as the deconvolution kernel is responsible for the fluence generation, the overall accuracy improvement of the new DC version in the presence of tissue inhomogeneity is not obvious. The ability of the DC to reconstruct the fluence of simple square fields was first tested in simple geometry. The accuracy of the entrance fluence reconstructed by the deconvolution kernel was assessed in both homogeneous and heterogeneous slab phantoms. Finally, the overall DC accuracy was evaluated on anthropomorphic phantom with VMAT plans.

The DC version 5.8 evaluated in this work is a standalone software version that is not commercially available anymore. The DC is now included in the 7.2 version of RadCalc software (Lifeline Software Inc., Tyler, TX, USA).

2.1. Slab Phantom Tests

The I'mRT Phantom (IBA Dosimetry, Schwarzenbruck, Germany), shown in Figure 1, consisting of slabs of RW3 material of nearly water equivalence, was used. Its central cubic insert was filled in three different ways: homogeneously with RW3 slabs (H configuration) or replacing the central slab with air and bone inserts (A and B configuration, respectively). Square fields with different sizes of 2, 3, 4, 6, 8, 10, 12, and 15 cm were calculated by Monaco 5.11.03 TPS (Elekta Oncology Systems, Crawley, UK) on the three phantom configurations by using 100 Monitor Units (MU) per beam. The beam isocenter was placed at the phantom center for all beams. The accuracy of the entrance fluence reconstructed by the deconvolution kernel algorithm was assessed by comparing the reconstructed entrance fluence of the square fields with the nominal fluence planned by the TPS and delivered.

Figure 1. I'mRT Phantom used for verification of the fluence reconstruction accuracy. On the left side, the homogenous slab phantom configuration is shown, in the central part the slab phantom with the air insert is shown, and on the left side the slab phantom with the bone insert is shown.

2.2. Anthropomorphic Phantom Tests

The Alderson Rando phantom (Alderson Research Laboratories, USA) was used for VMAT QA on the prostate, the head and the neck, the brain, and lung sites.

The CT scan of the phantom was acquired on GE Brightspeed equipment with the following parameters: 120 kV, 2.5 mm slice thickness, 100 mA/rot.

The phantom was contoured with the MIM Maestro (MIM Software, Inc., Cleveland, OH, USA) software version 6.7. In order to produce realistic planned dose distributions, contours from real treated patients, including target and organs at risk, were deformably registered on the phantom and then manually corrected to avoid registration artifacts. Contours used for planning are reported in Figure 2. The Monaco 5.11 TPS was used to optimize VMAT plans. Clinical templates were applied to generate the plans. The voxel size was $3 \times 3 \times 2.5$ mm^3. The dose prescriptions and planning specifications for each plan are reported in Table 1.

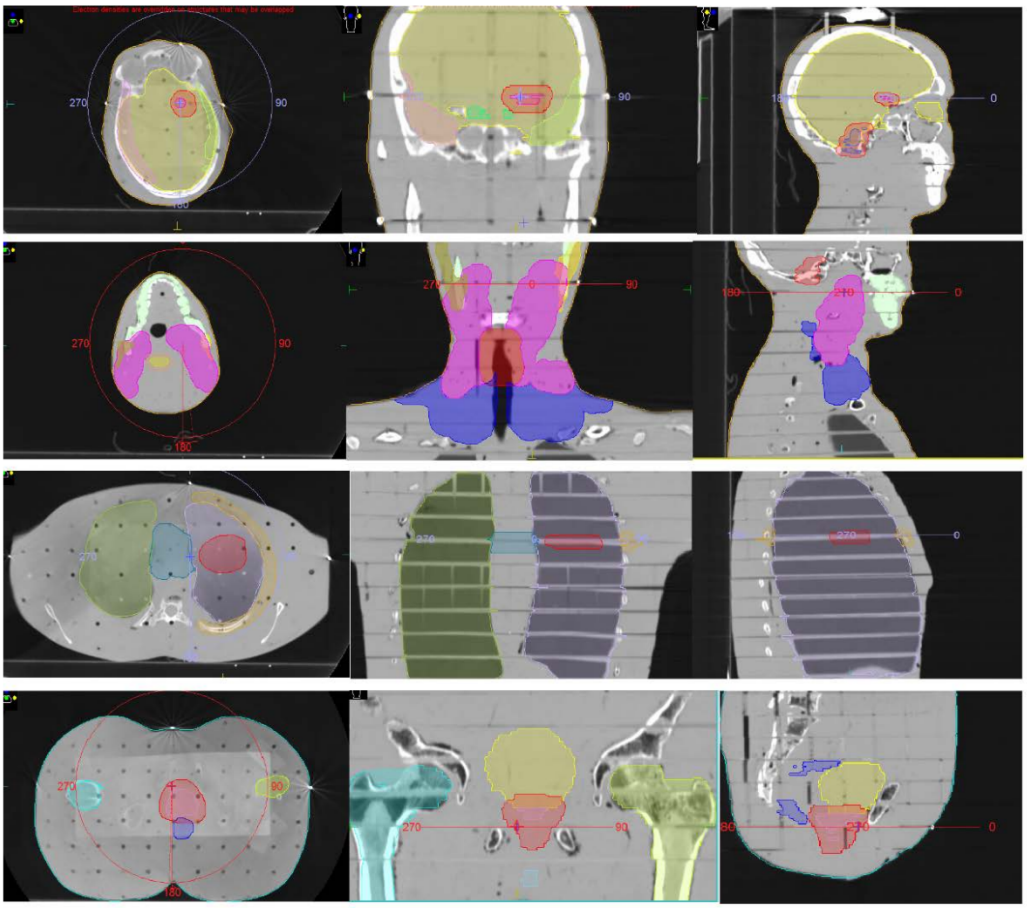

Figure 2. The Alderson phantom with the applied contours used for planning.

Table 1. Parameters used for planning the volumetric modulated treatment with the radiobiological cost functions of MONACO 5.11.

Plan	Arcs	Beam Energy	Tot MU	Structures Used in Plan Optimization	Dose Prescription Tot (frac) Gy
Prostate	One 360° arc	10 MV	896.3	PTV; CTV; Bladder; Rectum; Femoral Heads; Penil Bulb	70.2 (2.7)
Brain	One 360° arc	6 MV	324.1	PTV; CTV; Brain, Brainstem, Ocular Bulbs	24 (2)
Head and neck	Four 360° arcs	6 MV	838.1	PTV 70; PTV 60; PTV 54; Parotids glands; Cord; Brainstem	70–60–54 (2.1–1.8–1.7)
Lung	One 180° arc	6 MV	439.1	PTV; CTV; Lungs; Mediastinum; Chest wall	50 (2)

2.3. Plans Delivery

The linac Elekta Synergy, equipped with a multileaf collimator of 40 pairs of 1 cm wide leaves, was used for dose delivery. Each plan (square field or VMAT) was irradiated three times. Before irradiation, 3D volumetric imaging was acquired for set-up correction with a three translational degree-of-freedom robotic couch using the kV cone-beam CT (CBCT) XVI 5.1. For VMAT plans, before each irradiation, a Gafchromic® EBT3 film was inserted between two slices containing the isocenter point.

2.4. EPID Dosimetry

Transit images were acquired with the portal imaging system Iview-GT equipped with the software Iview-GT 3.4. The EPID acquisition was in cine mode for the VMAT beams and in IMRT mode for the square fields. A 10 × 10 cm^2 square field with 100 MU was used for calibration. For each irradiated plan (square field and VMAT), a 3D EPID reconstructed dose was generated with both the PB and the CCC algorithms. The voxel size for the DC doses was set at 1 × 1 mm^2 along the transverse axis and at 2 mm along the longitudinal axis.

2.5. Radiochromic Films Analysis

Gafchromic® EBT3 films (lot No. 09071703) were used with dimensions 25.4 × 20.3 cm^2. Films were digitized using an Epson Expression 10000 XL scanner in transmission mode. RGB positive images were collected at a depth of 16 bits per color channel and a spatial resolution of 72 dpi (pixel size 339 μm). Scanning was conducted through the Epson Scan driver and software settings were chosen to disable all color correction options. Transmission images were saved in TIFF.

A previously determined calibration curve (obtained for the same film lot) was applied. For the conversion of the film pixel value into dose, a multi-channel method was used. Details on film calibration and handling can be found in [16]. For film calibration and dose conversion, FilmQA™ Pro software (Ashland Inc., Wayne, NJ, USA) was used.

2.6. Dose Distributions Agreement Analysis

FilmQA™ Pro software was used for the film comparison with both TPS and DC dose distributions. Films were registered with TPS and DC dose maps by using marks placed on the film before irradiation and indicating the isocenter position. Gamma analysis was performed in a user-defined region of interest (ROI) (local gamma 3%/3 mm, threshold 10%).

The agreement between TPS computed and EPID reconstructed doses was assessed by evaluating 2D GAI in the coronal slice passing through the isocenter. GAI analysis was performed with the same software: FilmQA was used for EPID vs. film dose agreement in the same user-defined ROI and parameters. The reported GAI are the average values (+/−1 standard deviation) over the three irradiations.

3. Results

3.1. Slab Phantom Tests

The fluence reconstruction accuracy was tested in the slab phantom. The results of the irradiations with the slab phantom show that the fluence reconstruction is accurate (within 2%) in all slab configurations (Figure 3). In the homogeneous configuration, the fluence reconstructed by the deconvolution kernel was within 1% accuracy in most of the tested field's size: only the 3 × 3, the 4 × 4, and the 15 × 15 beams show discrepancies between 1% and 1.5%. The slab phantom with the air insert showed the worst result for the 3 × 3 field size, with a discrepancy of 1.9%; however, the overall accuracy is high, as all the other field sizes, except the 15 × 15, are below the 1% accuracy. With the bone inhomogeneity, the accuracy of fluence reconstruction is similar to the homogeneous phantom: only the 3 × 3 field size exhibits deviation greater than 1%, and all other field sizes are below the 1% threshold. As the new deconvolution kernel of the 5.8 DC version accurately produced the fluence in all phantom configurations, the final dose reconstruction accuracy of the DC 5.8, in the presence of inhomogeneities, is mainly dependent on the dose computation algorithm. In fact, as shown in Figure 4, the PB algorithm obtained the typical dose overestimates in the presence of air, and the CC algorithm obtained good results compared to the Monte Carlo TPS algorithm.

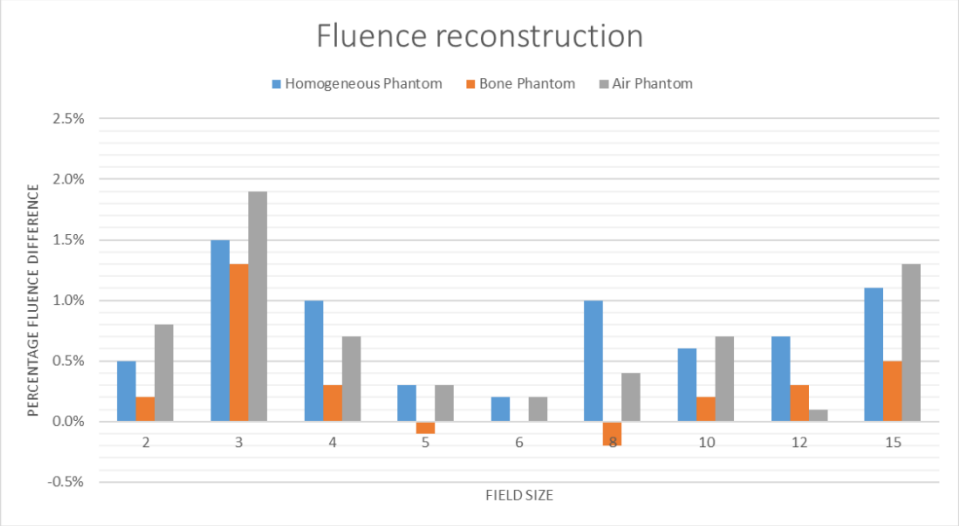

Figure 3. In this figure, the primary fluence reconstructed by the deconvolution kernel of DC in the slab phantom with homogeneous insert is shown with bone-like insert and with air insert.

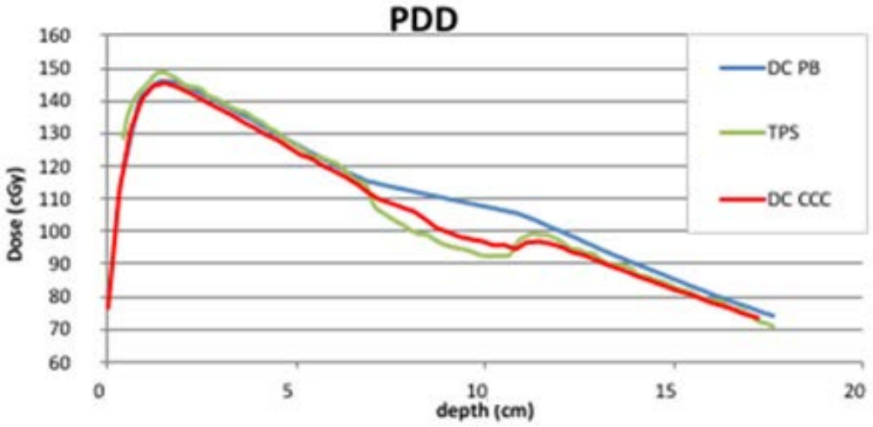

Figure 4. Percentage depth dose (PDD) on the slab phantom with air inhomogeneity on the central axis computed by the treatment planning system Monaco 5.11 with MonteCarlo algorithm and reconstructed with the pencil beam (PB) algorithm and the Collapsed Cone Convolution algorithm of the EPID algorithm Dosimetry Check 5.8.

3.2. Anthropomorphic Phantom Tests

The agreement between film measurements and TPS computed doses, DC reconstructed doses with PB, and DC reconstructed doses with CC algorithms, respectively, is reported in Figure 5. Overall, the film measurements and TPS data show a good agreement: the best results were found for brain plans (96.5%) and for prostate plans (94.3%), while for lung and head and neck plans, the agreement was, respectively, 90.0% and 91.3% (at 3%/3 mm 2D local gamma comparison, threshold 10%). The agreement between film and EPID is shown in Figures 5 and 6. In all anatomical sites except the lung, the GAI of film vs. DC doses was high and very similar for both the PB and the CCC algorithms. The best agreement was found in the head and the neck (98.6% for the PB algorithm and 96.6% for the CCC). In the brain, the agreement was 94.6% for the CC algorithm and 94.1% for the PB, in prostate plans it was 92.7% for the CC and 93.2% for the PB, and a large drop was observed for lung plans where the agreement was 93.9% for the CC and only 54.1% for the PB.

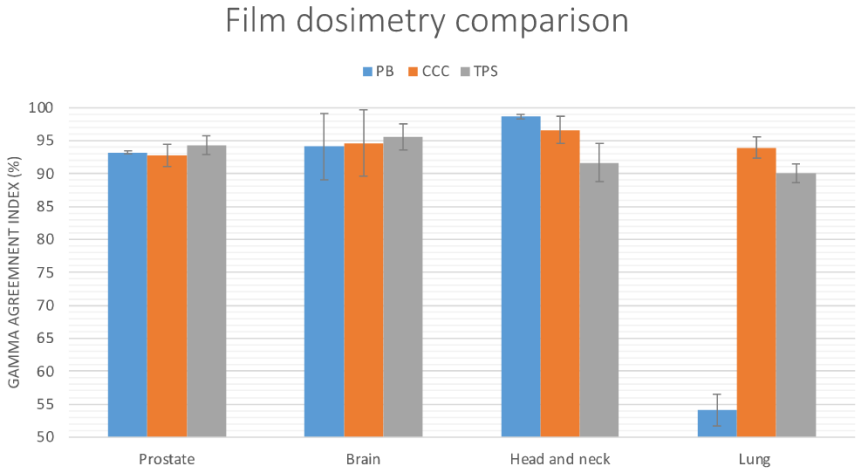

Figure 5. Gamma agreement index at 3%/3 mm local normalization with 10% dose threshold between film dosimetry at the central axial slice, the two Dosimetry Check algorithms, pencils beam (PB) and Collapsed Cone Convolution (CCC), and the planned dose distributions computed by the treatment planning system (TPS).

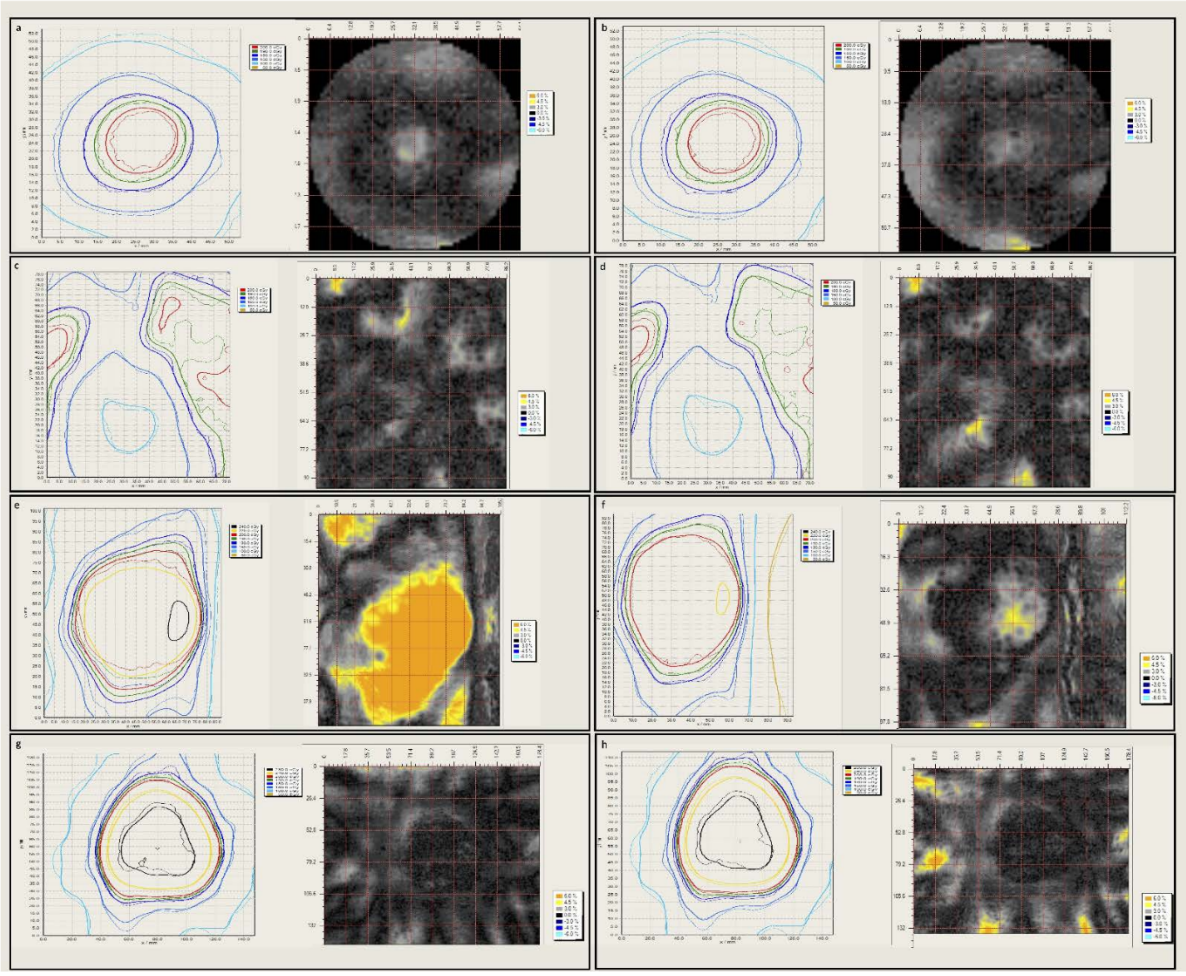

Figure 6. Isodose lines comparison (DC in bold and EBT3 in thin) and map of the gamma values (local, 3%/3 mm, threshold 10%) for the different considered treatment sites and calculation algorithms. (**a**) Brain plan and PB calculation algorithm; (**b**) Brain plan and CC calculation algorithm; (**c**) H&N plan and PB calculation algorithm; (**d**) H&N plan and CC calculation algorithm; (**e**) Lung plan and PB calculation algorithm; (**f**) Lung plan and CC calculation algorithm; (**g**) Prostate plan and PB calculation algorithm; (**h**) Prostate plan and CC calculation algorithm.

The agreement between DC and TPS is reported in Figures 7 and 8. The GAI was good for the DC doses reconstructed with the CC algorithm, while the PB algorithm results were less satisfactory. In the lung, as expected, the PB algorithm performed worse and the results of the comparisons with the TPS dose were not acceptable. Conversely, the CC obtained a good agreement with the calculated dose (94.7%). In the head and the neck, the PB algorithm GAI was 87.1% and the CC algorithm obtained a higher agreement (95.5%). In the brain, PB and CC algorithms obtained similar results: 93.5% vs. 93.8%. Finally, in the prostate, the PB GAI was 96.3% against the 99.6% obtained by the CC algorithm.

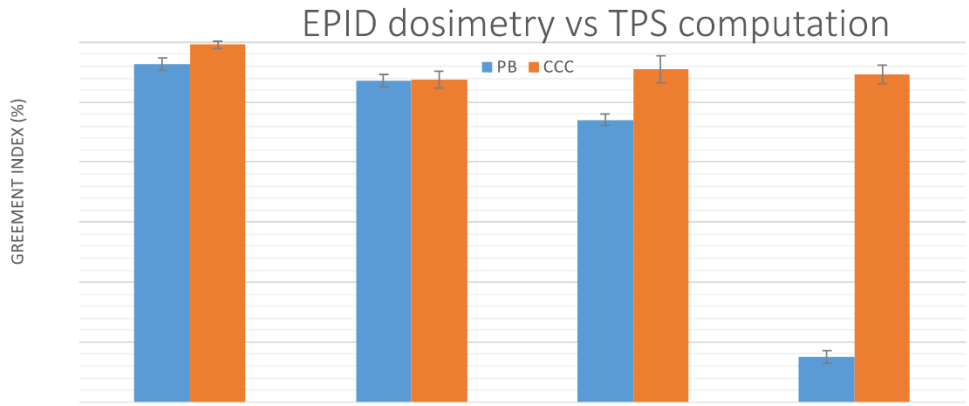

Figure 7. Gamma agreement index at 3%/3 mm local normalization with 10% dose threshold, in the axial slice passing through the isocenter, between the Dosimetry Check doses reconstructed with the two algorithms, pencils beam (PB) and Collapsed Cone Convolution (CCC), and the planned doses computed by the treatment planning system (TPS).

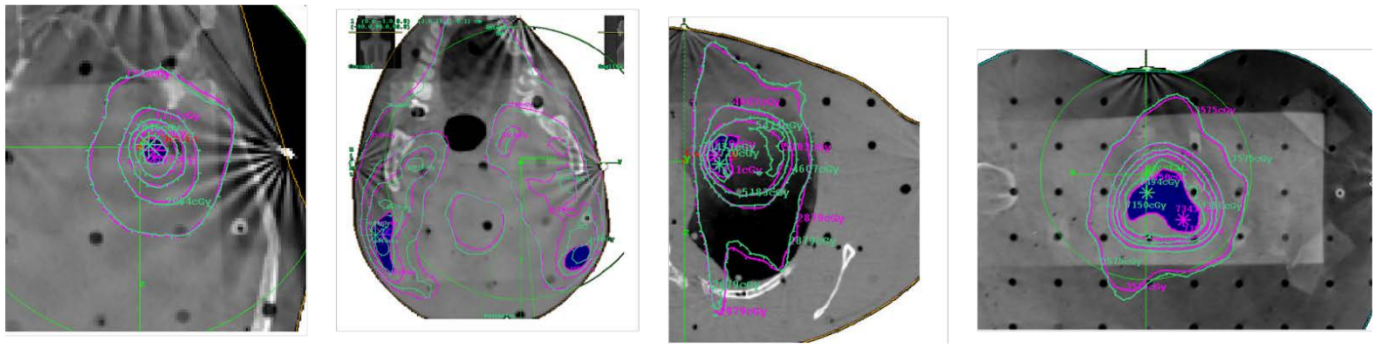

Figure 8. Comparison of computed dose distribution for the VMAT plans: green lines are the doses computed by the treatment planning system; pink lines are the doses reconstructed by the Dosimetry check with the Collapsed cone convolution algorithm. Isodoses curves displayed are the 100%, 95%, 90%, 80% and 50% of the prescribed dose.

4. Discussion

In this work, the accuracy of a novel EPID back-projection transit algorithm (DC 5.8) was assessed, to our knowledge, for the first time, against direct measurements with film dosimetry in an anthropomorphic phantom. The novel DC algorithm was tested in realistic geometries with inhomogeneous tissue densities. The tests performed in the slab phantom aimed to determine the accuracy of the entrance fluence reconstructed by the deconvolution kernel. For all the field sizes, the differences between the reconstructed MUs and the planned MUs are within 2%. The main finding of our work came from the direct comparison of the film measurements and EPID transit reconstructed doses. The GAI between the two measurements was very high, showing a high accuracy of the EPID reconstructed doses in anthropomorphic geometries. The PB algorithm of DC was already tested in a homogeneous phantom against the 2D ionization chamber array for

VMAT plans [4], and the agreement of the two measurements was high. However, the PB algorithm was not able to accurately reproduce the dose distributions in the lung, and a strategy of in-water re-computation was needed. The same "in aqua-vivo" solution was previously applied by Wendling et al. [17] to the EPID transit algorithm developed at NKI [18]. The novel CC algorithm of DC was otherwise shown to be able to accurately reproduce the dose distribution also in the lung. The dose reconstructed by DC with the CC algorithm can be directly compared with the TPS doses in the lung target without any need for in-water re-computation.

Van Uytven and co-workers [19] have reported the accuracy of the homemade PDR EPID back-projection algorithm in an anthropomorphic phantom against TPS computation. The dose distributions reconstructed by the PDR algorithm were also accurate in the presence of tissue inhomogeneity. However, in the work of Van Uytven, the EPID doses were only compared to the TPS doses computed by the AAA Eclipse algorithm. Even if the TPS computation could be highly accurate, after proper system commissioning, it should be viewed as only an estimate of the actual dose delivered by the linac. In fact, residual inaccuracies of the TPS implementation, and/or variability of the linac output due to leaves and collimators movement and positioning inaccuracy and mis-calibration, and to monitor unit mis-calibration, limit the use of the TPS computation as a gold standard. We believe that only a direct measure with film could be considered as a gold standard for evaluating the accuracy of an in vivo EPID system before clinical implementation. Radiochromic dosimetry is challenging, but currently, it is consolidated that proper handling, together with the application of a multichannel approach for dose calibration, allows for reliable results [16,20,21].

Our work has some limitations: the first is the phantom used. The Anderson Rando phantom was not originally designed for film dosimetry and offers the only possibility of measuring dose distributions with film between axial slices. This could create a certain space between slices that needs to be taken into account during the plan computation. Moreover, the presence of holes inside the phantom, designed for point dosimetry with thermoluminescent detectors, could add unnecessary complexity to the EPID algorithm. With this work, we highlighted the necessity to develop dedicated anthropomorphic phantoms that could be used for validating the EPID dosimetry with film inserted in multiple planes.

As a future development of this study, we are planning to include more anatomical sites and the evaluation of the sensitivity analysis to error detection, again in combination with film dosimetry.

5. Conclusions

In this work, we validated a novel algorithm for EPID in vivo dosimetry. The fluence reconstruction resulted within 2% in both the homogeneous and the inhomogeneous slab phantoms. The algorithm accuracy for VMAT treatment was tested against a direct film measurement in an anthropomorphic phantom in different anatomic sites. The GAI between DC and film was 92.7% in the prostate, 92.9% in the lung, 96.6% in the head and the neck, and 94.6% in the brain. The methods used in this work can be applied to any EPID back-projection algorithm for in vivo applications.

Author Contributions: Conceptualization, M.E., L.M., S.R. and C.T.; Methodology, M.E., L.M. and C.T.; Validation, E.V., S.P. and C.T.; Formal Analysis, M.E. and L.M.; Investigation, M.E. and L.M.; Resources, M.E., L.M. and C.T.; Data Curation, M.E., L.M., E.V., S.R., S.P. and C.T.; Writing—Original Draft Preparation, M.E. and L.M.; Writing, Review and Editing, M.E., L.M., E.V., S.R., S.P. and C.T.; Visualization, M.E., L.M., E.V., S.R., S.P. and C.T.; Supervision, C.T. All authors have read and agreed to the published version of the manuscript.

Funding: This research received no external funding.

Institutional Review Board Statement: Not applicable.

Informed Consent Statement: Not applicable.

Data Availability Statement: Not applicable.

Conflicts of Interest: The authors declare no conflict of interest.

References

1. International Atomic Energy Agency. *Development of Procedures for In Vivo Dosimetry in Radiotherapy*; IAEA Human Health Report No. 8; IAEA: Vienna, Austria, 2013.
2. COUNCIL DIRECTIVE 2013/59/EURATOM of 5 December 2013. Available online: https://eur-lex.europa.eu/eli/dir/2013/59/oj (accessed on 5 November 2021).
3. Esposito, M.; Villaggi, E.; Bresciani, S.; Cilla, S.; Falco, M.D.; Garibaldi, C.; Russo, S.; Talamonti, C.; Stasi, M.; Mancosu, P. Estimating dose delivery accuracy in stereotactic body radiation therapy: A review of in-vivo measurement methods. *Radiother. Oncol.* **2020**, *149*, 158–167. [CrossRef] [PubMed]
4. Esposito, M.; Bruschi, A.; Bastiani, P.; Ghirelli, A.; Pini, S.; Russo, S.; Zatelli, G. Characterization of EPID software for VMAT transit dosimetry. *Australas. Phys. Eng. Sci. Med.* **2018**, *41*, 1021–1027. [CrossRef] [PubMed]
5. Arilli, C.; Wandael, Y.; Galeotti, C.; Marrazzo, L.; Calusi, S.; Grusio, M.; Desideri, I.; Fusi, F.; Piermattei, A.; Pallotta, S.; et al. Combined Use of a Transmission Detector and an EPID-Based In Vivo Dose Monitoring System in External Beam Whole Breast Irradiation: A Study with an Anthropomorphic Female Phantom. *Appl. Sci.* **2020**, *10*, 7611. [CrossRef]
6. Esposito, M.; Ghirelli, A.; Pini, S.; Alpi, P.; Barca, R.; Fondelli, S.; Leonulli, B.G.; Paoletti, L.; Rossi, F.; Bastiani, P.; et al. Clinical implementation of 3D in vivo dosimetry for abdominal and pelvic stereotactic treatments. *Radiother. Oncol.* **2021**, *154*, 14–20. [CrossRef] [PubMed]
7. Bossuyt, E.; Weytjens, R.; Nevens, D.; De Vos, S.; Verellen, D. Evaluation of automated pre-treatment and transit in-vivo dosimetry in radiotherapy using empirically determined parameters. *Phys. Imaging Radiat. Oncol.* **2020**, *16*, 113–129. [CrossRef] [PubMed]
8. *ICRU: Prescribing, Recording, and Reporting Photon-Beam Intensity-Modulated Radiation Therapy (IMRT)*; ICRU Report 83, J. ICRU; Oxford University Press: Oxford, UK, 2010; Volume 10.
9. Esposito, M.; Piermattei, A.; Bresciani, S.; Orlandini, L.C.; Falco, M.D.; Giancaterino, S.; Cilla, S.; Ianiro, A.; Nigro, R.; Botez, L.; et al. Improving dose delivery accuracy with EPID in vivo dosimetry: Results from a multicenter study. *Strahlenther. Und Onkol.* **2021**, *197*, 633–643. [CrossRef] [PubMed]
10. Mijnheer, B.J.; González, P.; Olaciregui-Ruiz, I.; Rozendaal, R.A.; van Herk, M.; Mans, A. Overview of 3-year experience with large-scale electronic portal imaging device–based 3-dimensional transit dosimetry. *Pract. Radiat. Oncol.* **2015**, *5*, e679–e687. [CrossRef] [PubMed]
11. Hanson, I.; Hansen, V.N.; Olaciregui-Ruiz, I.; van Herk, M. Clinical implementation and rapid commissioning of an EPID basedin-vivodosimetry system. *Phys. Med. Biol.* **2014**, *59*, N171–N179. [CrossRef] [PubMed]
12. Olaciregui-Ruiz, I.; Vivas-Maiques, B.; Kaas, J.; Perik, T.; Wittkamper, F.; Mijnheer, B.; Mans, A. Transit and non-transit 3D EPID dosimetry versus detector arrays for patient specific QA. *J. Appl. Clin. Med. Phys.* **2019**, *20*, 79–90. [CrossRef] [PubMed]
13. Chendi, A.; Botti, A.; Orlandi, M.; Sghedoni, R.; Iori, M.; Cagni, E. EPID-based 3D dosimetry for pre-treatment FFF VMAT stereotactic body radiotherapy plan verification using dosimetry CheckTM. *Phys. Med.* **2021**, *81*, 227–236. [CrossRef] [PubMed]
14. Olaciregui-Ruiz, I.; Beddar, S.; Greer, P.; Jornet, N.; McCurdy, B.; Paiva-Fonseca, G.; Mijnheer, B.; Verhaegen, F. In vivo dosimetry in external beam photon radiotherapy: Requirements and future directions for research, development, and clinical practice. *Phys. Imaging Radiat. Oncol.* **2020**, *15*, 108–116. [CrossRef] [PubMed]
15. Papanikolaou, N.; Stathakis, S. Dose-calculation algorithms in the context of inhomogeneity corrections for high energy photon beams. *Med. Phys.* **2009**, *36*, 4765–4775. [CrossRef] [PubMed]
16. Marrazzo, L.; Zani, M.; Pallotta, S.; Arilli, C.; Casati, M.; Compagnucci, A.; Talamonti, C.; Bucciolini, M. GafChromic® EBT3 films for patient specific IMRT QA using a multichannel approach. *Phys. Med.* **2015**, *31*, 1035–1042. [CrossRef] [PubMed]
17. Wendling, M.; McDermott, L.N.; Mans, A.; Sonke, J.-J.; Stroom, J.; van Herk, M.; Mijnheer, B.J. In aqua vivo EPID dosimetry. *Med. Phys.* **2011**, *39*, 367–377. [CrossRef] [PubMed]
18. Wendling, M.; Louwe, R.J.W.; McDermott, L.N.; Sonke, J.-J.; Van Herk, M.; Mijnheer, B.J. Accurate two-dimensional IMRT verification using a back-projection EPID dosimetry method. *Med. Phys.* **2006**, *33*, 259–273. [CrossRef] [PubMed]
19. Van Uytven, E.; Van Beek, T.; McCowan, P.M.; Chytyk-Praznik, K.; Greer, P.; McCurdy, B.M.C. Validation of a method for in vivo 3D dose reconstruction for IMRT and VMAT treatments using on-treatment EPID images and a model-based forward-calculation algorithm. *Med. Phys.* **2015**, *42*, 6945–6954. [CrossRef] [PubMed]
20. Micke, A.; Lewis, D.F.; Yu, X. Multichannel film dosimetry with nonuniformity correction. *Med. Phys.* **2011**, *38*, 2523–2534. [CrossRef] [PubMed]
21. Lewis, D.; Micke, A.; Yu, X.; Chan, M.F. An efficient protocol for radiochromic film dosimetry combining calibration and measurement in a single scan. *Med. Phys.* **2012**, *39*, 6339–6350. [CrossRef] [PubMed]